

Controlled Synthesis of TT Phase Niobium Pentoxide Nanowires Showing Enhanced Photocatalytic Properties

Kenji Saito and Akihiko Kudo*

Department of Applied Chemistry, Faculty of Science, Tokyo University of Science, 1-3 Kagurazaka, Shinjuku-ku, Tokyo 162-8601

Received March 2, 2009; E-mail: a-kudo@rs.kagu.tus.ac.jp

The controlled synthesis of niobia nanowires with TT (tief–tief) phase (TT-Nb_2O_5-NW) that is the stable phase at low temperature was accomplished through calcination of niobium-based amorphous nanowires (Nb_2O_5-NW) composed of closely packed primary particles, obtained by the reaction of water-soluble niobium oxo-oxalate complex $(NH_4)_3[NbO(Ox)_3]\cdot H_2O$ (Ox = oxalate) with trioctylamine (TOA) employed as a structure-directing agent. TT-Nb_2O_5-NW gave a sharp absorption edge, which agreed well with that of the same crystalline phase of bulk niobia (TT-Nb_2O_5-B), suggesting no influence on the band gap energies by the shape transformation. An aqueous suspension containing TT-Nb_2O_5-NW and a sacrificial reagent was irradiated with white light ($\lambda > 300$ nm) from a Xe lamp to afford the enhanced photocatalytic activities for H_2 or O_2 evolution compared with that of conventional TT-Nb_2O_5-B.

Since the discovery of water splitting into H_2 and O_2 using a titanium dioxide photoelectrode by Honda and Fujishima in 1972,[1] considerable efforts have so far been devoted to develop powder photocatalysts that are active for H_2 and/or O_2 production to achieve solar water splitting systems, enabling us to deal more effectively with environmental issues caused by the use of fossil fuels.[2] Among the variety of methods for enhancement of photocatalytic properties reported to date,[3] the metal ion doping of photocatalysts has merited special attention due to morphological changes suitable for separation of two-electron reduction and four-electron oxidation sites as represented by La-doped $NaTaO_3$.[4] However, such doping method largely depends on the host materials. This prompts us to design the metal oxide nanotubes and nanowires, because they possess unique chemical and physical properties depending on their length and diameters that have been revealed by a number of potential applications.[5] Although a few reports with regard to the utilization of semiconductor nanowires for photocatalytic H_2 or O_2 evolution have so far been reported, the enhancement of photocatalytic properties is still a significant challenge because of the minimum requirement of high crystallinity to promote the efficient photogenerated carrier transfer from bulk to surface associated with inhibition of charge recombination process following light irradiation.[6] We report herein our recent discovery that the niobium complex-based synthesis of niobia nanowires with TT phase (TT-Nb_2O_5-NW) in the structure directing agent affords high crystallinity and such nanowires exhibited enhanced photocatalytic activities for H_2 and O_2 evolution compared with that of bulk TT-Nb_2O_5-B, under ultraviolet light illumination.

Experimental

All solvents and chemicals were reagent grade qualities and used without further purification. The niobium complex, $(NH_4)_3[NbO(Ox)_3]\cdot H_2O$, was prepared according to previously reported procedures.[7] Amorphous niobia nanowires (Nb_2O_5-NW) and crystalline niobia nanowires with a TT phase (TT-Nb_2O_5-NW) were synthesized as follows: the niobium complex was mixed with trioctylamine, denoted as TOA (the ratio of $(NH_4)_3[NbO(Ox)_3]\cdot H_2O$ with TOA was fixed to 1.0 g/25 mL), in a 200-mL round-bottom flask equipped with a condenser.[8] The mixture was heated at a rate of 275 K min^{-1}, followed by maintaining at 573 K for 2.5 h. The pale yellow precipitates were filtered off, washed several times with ethanol and water, and dried at 333 K for several hours to obtain Nb_2O_5-NW. Nb_2O_5-NW was then simply calcinated at a rate of 280 K min^{-1} using an electric furnace and maintained at 773 K for 5 h, resulting in the formation of TT-Nb_2O_5-NW.

The $Nb_2O_5\cdot xH_2O$ used as a precursor for bulk TT-Nb_2O_5 (TT-Nb_2O_5-B) was prepared by hydrolyzing $K_8Nb_6O_{19}$ that was obtained by melting a mixture of KOH (10.3 g, 184 mmol) and Nb_2O_5 (4.9 g, 18.4 mmol) in a Ni crucible at 653 K for 5 h. The $Nb_2O_5\cdot xH_2O$ powder was then calcinated at 773 K for 2 h to obtain TT-Nb_2O_5-B.

The Nb_2O_5-NW and TT-Nb_2O_5-NW powders were characterized by powder X-ray diffraction (Rigaku; Miniflex, Cu Kα). Scanning electron microscope (SEM) images were taken using a JEOL JSM-6700F. Transmission electron microscope (TEM) images were collected on a HITACHI 9500 operating at an accelerating voltage of 200 kV. TEM samples were typically prepared from a diluted ethanol suspension to minimize aggregation between nanowires during the gradual evaporation of solvent. BET surface area and porosity of the samples were measured with a Coulter SA 3100 apparatus using nitrogen as an adsorbing gas. IR spectra were obtained with a Fourier transform IR (FT/IR-4100, Jasco) spectrometer equipped with a mercury cadmium telluride (MCT) detector. Diffuse reflection spectra were recorded on a UV–vis–NIR spectrometer (JASCO; UbestV-570) and were converted from reflection to absorbance by the Kubelka–Munk method.

Photocatalytic reactions were carried out in a reaction cell with top a window made of Pyrex, which was connected to a gas-closed circulation system with online gas chromatograph to analyze the gaseous products. In a typical procedure, the photocatalyst powder

Published on the web August 7, 2009; doi:10.1246/bcsj.82.1030

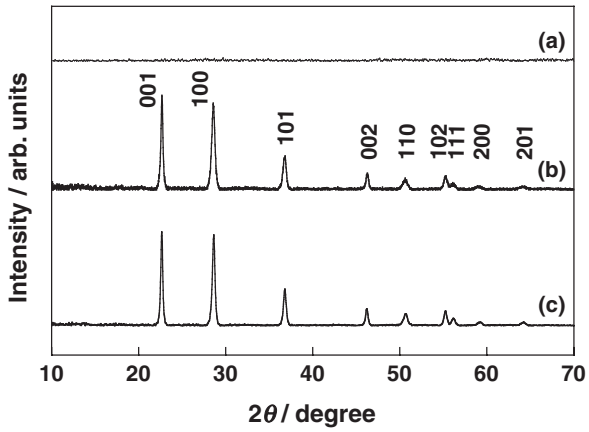

Figure 1. X-ray diffraction patterns of (a) Nb_2O_5-NW, (b) TT-Nb_2O_5-NW, and (c) TT-Nb_2O_5-B.

(0.1 g) was dispersed with a magnetic stirrer in 120 or 150 mL of an aqueous solution containing a sacrificial reagent such as methanol or silver nitrate at 293 K. Argon gas (40 Torr) was introduced into the system after deaeration. A 300-W Xe-arc lamp (Perkin-Elmer: Cermax-PE300BF) was employed for light irradiation ($\lambda > 300$ nm). Pt, Ru, and Rh cocatalysts for H_2 evolution were deposited on photocatalysts using a conventional photodeposition method from H_2PtCl_6, $RuCl_3$, and $RhCl_3$ as the metal sources in situ. Apparent quantum yields (A.Q.Y.) were measured using a 300-W Xe illuminator (ASAHI SPECTRA; MAX-301) with a band-pass filter (ASAHI SPECTRA) as an excitation source and actinometer. The A.Q.Y. was determined according to the eq 1:

$$\text{A.Q.Y. (\%)} = \frac{\text{The number of reacted electrons}}{\text{The number of incident photons}} \times 100 = \frac{\text{The number of evolved } H_2 \text{ molecules} \times 2}{\text{The number of incident photons}} \times 100 \quad (1)$$

Results and Discussion

Synthesis and Characterization. The crystal structures of Nb_2O_5-NW and TT-Nb_2O_5-NW prepared by the calcination of Nb_2O_5-NW at 773 K were determined by X-ray diffraction (XRD) patterns as shown in Figure 1. Nb_2O_5-NW showed no characteristic signal, indicating an amorphous structure.

In contrast, the diffraction peaks of TT-Nb_2O_5-NW were indexed with the pseudo-hexagonal Nb_2O_5 phase (lattice constants are: $c = 3.925$ Å and $a = 3.607$ Å).[9] It has been reported that the first crystalline TT phase of niobia appears during the heating of amorphous precursors at temperature of 713 K.[9b] The SEM images of Nb_2O_5-NW clearly indicated the homogeneous nanowire morphology with diameters 30–50 nm and lengths up to several micrometers as shown in Figures 2a and 2b, in contrast to spherical particles of $Nb_2O_5 \cdot nH_2O$ and TT-Nb_2O_5-B (Figure S1). The short nanowires were also observed as a minor species (Figure 2d). These were assigned to the intermediate in the course of the nanowire growth. The image of TT-Nb_2O_5-NW was virtually the same as compared with that of Nb_2O_5-NW as shown in Figure 2c, suggesting crystallization while maintaining their intrinsic morphologies. The energy dispersive spectrum of TT-Nb_2O_5-NW showed two

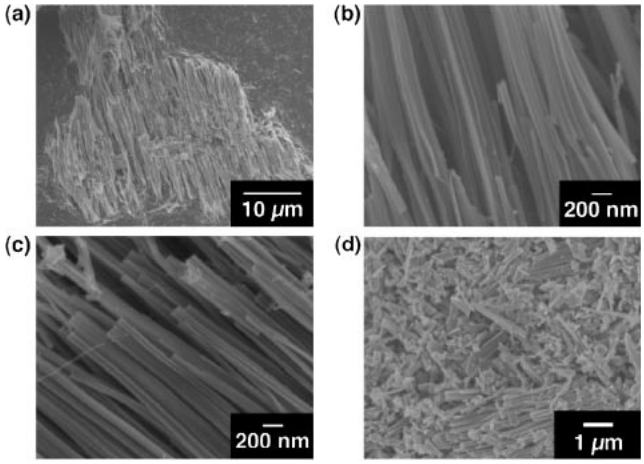

Figure 2. SEM images of (a) Nb_2O_5-NW, (b) magnified view of (a), (c) TT-Nb_2O_5-NW, and (d) short nanowires observed in Nb_2O_5-NW.

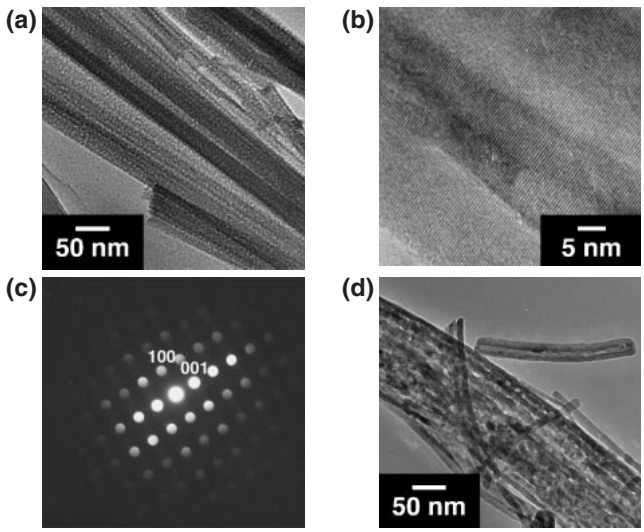

Figure 3. (a) TEM image of Nb_2O_5-NW, (b) HRTEM image of TT-Nb_2O_5-NW, (c) Electron diffraction pattern of TT-Nb_2O_5-NW, and (d) TEM image of TT-Nb_2O_5-NW showing tubular morphology.

peaks corresponding to the niobium and oxygen elements, indicating that no impurities existed in the sample. The TEM images of Nb_2O_5-NW indicated a nanowire structure composed of closely packed primary particles as seen in Figure 3a. On the other hand, the high-resolution TEM (HRTEM) image of TT-Nb_2O_5-NW showed clear lattice fringes perpendicular to growth direction, and the width of the fringes was 3.9 ± 0.2 Å, which corresponds to (001) crystal plane (Figure 3b). The electron diffraction pattern shown in Figure 3c further proved these nanowires to be single crystalline niobia. The TEM characterization of TT-Nb_2O_5-NW presented additional interesting results, i.e., tubular morphology, as shown in Figure 3d. The pore size distribution, based on the Barret, Joyner, and Halenda (BJH) theory, is shown in Figure S2 to verify the existence of nanotubes in the TT-Nb_2O_5-NW sample. As a result, TT-Nb_2O_5-NW exhibited a comparatively narrow distribution with ca. 6 nm of most frequent diameter, which agreed

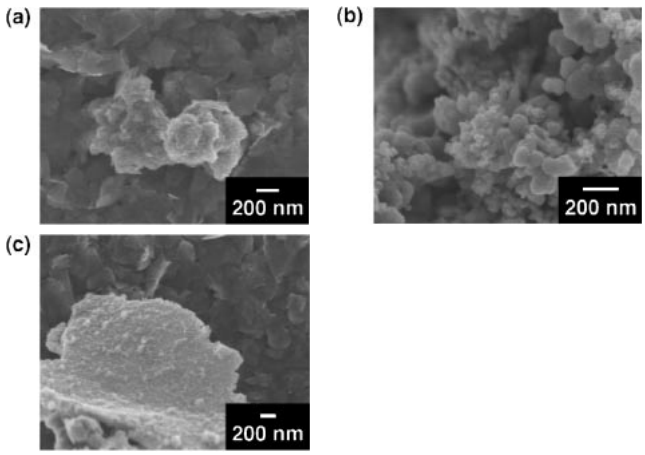

Figure 4. SEM images of the products given by the reaction of (a) $Nb(HC_2O_4)_5$ with TOA, (b) $Nb_2O_5 \cdot nH_2O$ with TOA, and (c) $(NH_4)_3[NbO(Ox)_3] \cdot H_2O$ with trimethylamine hydrochloride, under heat treatment of 573 K for 2.5 h.

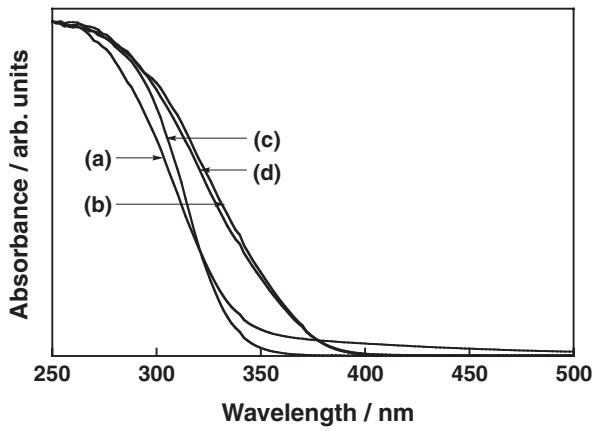

Figure 5. Diffuse reflection spectra of (a) Nb_2O_5-NW, (b) TT-Nb_2O_5-NW, (c) $Nb_2O_5 \cdot nH_2O$, and (d) TT-Nb_2O_5-B.

well with that observed in Figure 3d. In the case of Nb_2O_5-NW, ca. 3 nm nanopores existed in the sample and this may arise from the aperture between primary particles. The data for TT-Nb_2O_5-NW will raise a question of a definite amount of tubular structures in the sample. However, the strong aggregation between TT-Nb_2O_5-NW has precluded clear detection as an individual nanorod structure. To note the mechanistic insight into Nb_2O_5-NW formation, several control experiments were carried out. SEM images revealed that the combinations of the water-soluble niobium compounds ($Nb_2O_5 \cdot nH_2O$ and $Nb(HC_2O_4)_5$) with TOA and $(NH_4)_3[NbO(Ox)_3] \cdot H_2O$ with trimethylamine hydrochloride under identical conditions gave all small particles (Figure 4). Thus, the nanowire growth will be briefly interpreted as follows: TOA coordinates to the niobium complex associated with dissociation of oxalate ligand under heat treatment below the decomposition temperature of oxalic acid, followed by self-assembly to each other via the hydrophobic interaction between methylene groups in TOA.[10] The assembly then undergoes directional growth forming nanowire structures by heating above the decomposition temperature of oxalic acid to form Nb_2O_5-NW.

Figure 5 shows the diffuse reflection spectra of Nb_2O_5-NW, TT-Nb_2O_5-NW, $Nb_2O_5 \cdot nH_2O$, and TT-Nb_2O_5-B. The absorption spectrum of Nb_2O_5-NW gave a sharp absorption edge at 3.6 eV, which agreed well with that of $Nb_2O_5 \cdot nH_2O$, in addition to a long tail in the visible region. The observed tail may originate from the residual or decomposed alkyl chains in the Nb_2O_5-NW sample, judging from the IR spectra displaying the antisymmetric or symmetric stretching mode of ν_{as}(C–O), ν_{as}(C=O), ν_s(C=O), ν_1(N–H), and ν_3(N–H), shown in Figure S3.[11] Here, such organic compounds may affect the activities for photocatalytic reactions, and thus, we checked the IR spectrum of TT-Nb_2O_5-NW to show no existence of any detectable organic residuals (Figure S3c). TT-Nb_2O_5-NW and TT-Nb_2O_5-B exhibited the same absorption features as shown in Figures 5b and 5d, respectively, indicating no influence on the band gap by shape transformation. The difference in the band gap between amorphous and crystallized structure arises from the quantum size effect due to the small size of crystallite in amorphous structure as compared to that of crystal.

Photocatalytic Properties. Photocatalytic experiments were carried out to confirm if the band gap transitions seen in Figure 5 contribute to the H_2 or O_2 evolution under light irradiation. Niobia photocatalysts are known to show photocatalytic activities.[12] The photocatalytic reactions of TT-Nb_2O_5-NW and TT-Nb_2O_5-B are summarized in Table 1 with band gap and surface area. When optimized amounts of cocatalysts were loaded on the photocatalysts, the photocatalytic activities to reduce water to form H_2 were effectively enhanced for TT-Nb_2O_5-NW and TT-Nb_2O_5-B. The most important difference between the two photocatalysts lied in the absence of cocatalysts. TT-Nb_2O_5-B showed a negligible ability of 0.1 μmol h^{-1} whereas TT-Nb_2O_5-NW showed 10-fold greater activity (1.3 μmol h^{-1}). Furthermore, the maximum photocatalytic activity of Pt(1.0 wt %)/TT-Nb_2O_5-NW was clearly enhanced, compared to that of Pt(0.5 wt %)/TT-Nb_2O_5-B. The improved photocatalytic activities were also found in O_2 evolution reactions as shown in Figure 6. Thus, these results suggest that the structural conversion of spherical particles (TT-Nb_2O_5-B) into nanowires (TT-Nb_2O_5-NW) can offer the opportunity for enhancement of the photocatalytic activity for photoinduced reduction or oxidation of water.

To examine the influence of wavelength on photocatalytic H_2 evolution, we have measured an action spectrum of Pt(1 wt %)/TT-Nb_2O_5-NW as shown in Figure 7. The onset of the spectrum agreed well with that of the diffuse reflectance spectrum, indicating that the photocatalytic reaction proceeded with band gap transition. The observed photoresponse increased with going to shorter wavelength to attain 4.7% of an apparent quantum yield at 270 nm, and this value was clearly higher than 2.5% for Pt(0.5 wt %)/TT-Nb_2O_5-B.

The reason for the difference in photocatalytic properties between spherical particles and nanowires could be explained by considering the contribution of the following four factors: (i) crystallinity, (ii) structural anisotropy, (iii) surface area, and (iv) grain boundary. The high crystallinity promotes the efficient transfer of photogenerated carriers from bulk to surface associated with inhibition of charge recombination process. The crystallinity was found to be different in the two photocatalysts (the half-width for (001) diffraction was 0.26°

Table 1. Photocatalytic H_2 Evolution from 10 vol % of an Aqueous Methanol Solution over TT-Nb_2O_5-NW and TT-Nb_2O_5-B[a)]

Catalyst	Band gap	Cocatalyst	Surface area /$m^2\,g^{-1}$	Rate of H_2 evolution /$\mu mol\,h^{-1}$
TT-Nb_2O_5-NW[b)]	3.3	—	63	1.3
TT-Nb_2O_5-NW[b)]	3.3	Pt(0.5 wt %)	63	33
TT-Nb_2O_5-NW[b)]	3.3	Pt(0.7 wt %)	63	43
TT-Nb_2O_5-NW[b)]	3.3	Pt(1.0 wt %)	63	57
TT-Nb_2O_5-NW[b)]	3.3	Pt(1.5 wt %)	63	53
TT-Nb_2O_5-NW[b)]	3.3	Pt(2.0 wt %)	63	41
TT-Nb_2O_5-NW[b)]	3.3	Rh(1.0 wt %)	63	36
TT-Nb_2O_5-NW[b)]	3.3	Ru(1.0 wt %)	63	4.7
TT-Nb_2O_5-NW[c)]	3.3	Pt(1.0 wt %)	64	58
TT-Nb_2O_5-NW[d)]	3.3	Pt(1.0 wt %)	70	68
TT-Nb_2O_5-B	3.3	—	32	0.1
TT-Nb_2O_5-B	3.3	Pt(0.3 wt %)	32	13
TT-Nb_2O_5-B	3.3	Pt(0.5 wt %)	32	35
TT-Nb_2O_5-B	3.3	Pt(0.7 wt %)	32	12
TT-Nb_2O_5-B	3.3	Pt(1.0 wt %)	32	25
TT-Nb_2O_5-B	3.3	Pt(1.5 wt %)	32	29
TT-Nb_2O_5-B	3.3	Rh(0.5 wt %)	32	8.7
TT-Nb_2O_5-B	3.3	Ru(0.5 wt %)	32	trace

a) Reaction conditions: catalyst, 0.1 g; reactant solution; 150 mL; light source, 300-W Xe-arc lamp ($\lambda > 300$ nm); cell, top-irradiation cell with a Pyrex glass window. TT-Nb_2O_5-NW prepared under the following conditions: b) calcination of Nb_2O_5-NW at 773 K for 5 h with a heating rate of 280 K min^{-1}, c) calcination of Nb_2O_5-NW at 773 K for 5 h with a heating rate of 275 K min^{-1}, and d) calcination of Nb_2O_5-NW at 733 K for 12 h with a heating rate of 280 K min^{-1}. The half-width for (001) diffraction in the XRD patterns are 0.26, 0.30, and 0.29.

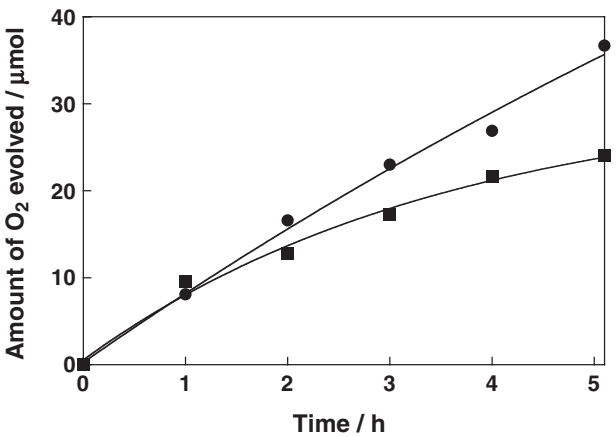

Figure 6. O_2 evolution from an aqueous silver nitrate solution (0.02 mol L^{-1}) over TT-Nb_2O_5-NW (●) and TT-Nb_2O_5-B (■). Conditions: catalyst, 0.1 g; light source, 300-W Xe lamp; reaction cell, top-irradiation cell with Pyrex glass window.

for TT-Nb_2O_5-NW and 0.32° for TT-Nb_2O_5-B, respectively) as recognized shown in Figure 1, and hence, the first factor (i) would contribute to this matter, i.e., the enhancement of the photocatalytic properties of TT-Nb_2O_5-NW compared to that of

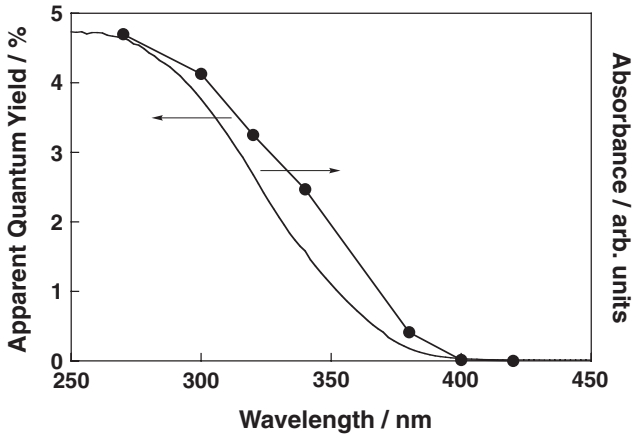

Figure 7. Action spectrum for H_2 evolution from an aqueous 10 vol % methanol solutions over Pt(1 wt %)-loaded TT-Nb_2O_5-NW.

TT-Nb_2O_5-B. The anisotropic strain would cause the same effect as (i) and is expected to contribute to the enhanced photocatalytic activities. The large surface area enhances the physical adsorption of reactants and the dispersibility of the powdered photocatalysts. Actually, TT-Nb_2O_5-NW gave approximately 2 times larger surface area than TT-Nb_2O_5-B, regardless of the same calcination temperature, as shown in Table 1. In addition, we have also examined how contributions from surface area affect the photocatalytic properties of TT-Nb_2O_5-NW. The surface area of TT-Nb_2O_5-NW could be somewhat controlled by considering the rate of phase transformation, and as expected, the amount of H_2 evolved correlated to the surface area (Table 1). These results indicate the definitive contribution of the surface area to enhancement of photocatalytic gas evolution on the nanowire structure. The grain boundary is known to function as recombination center of the photogenerated carrier. A SEM image of TT-Nb_2O_5-B powder shown in Figure S1 suggests that the small particles were strongly connected to each other and this would cause such grain boundary, in contrast to the case of TT-Nb_2O_5-NW (Figure 2c).

In summary, we have developed nanowire-shaped niobia photocatalysts that show enhanced activities for H_2 and O_2 evolution in the presence of sacrificial reagents, compared to spherical particles of conventional niobia with the same crystalline phase. Because the niobia nanowires obtained possess higher crystallinity than bulk niobia with the same TT phase regardless of the same calcination temperature, this complex-based synthesis enables us to afford semiconductor nanowires with high crystallinity. The syntheses of niobia nanowires and nanotubes have so far been pioneered by several groups,[13] however, nanowire-shaped powder photocatalysts possessing enhanced photocatalytic properties will play a pivotal role for further developing efficient visible light driven photocatalysts in combination with band engineering techniques.[2]

We gratefully acknowledge Prof. Hashimoto and Mr. Kuramochi for the HRTEM measurements in the department of physics, Tokyo University of Science. This work was

partially supported by a Grant-in-Aid for Young Scientists B (No. 20750113) from the Ministry of Education, Culture, Sports, Science and Technology (MEXT) of Japan, the Sumitomo Foundation, and the Mitsubishi Chemical Corporation Fund.

Supporting Information

SEM images of $Nb_2O_5 \cdot nH_2O$ and TT-Nb_2O_5-B (Figure S1), the pore-size distribution of Nb_2O_5-NW and TT-Nb_2O_5-NW (Figure S2), IR spectra of $(NH_4)_3[NbO(Ox)_3] \cdot H_2O$, Nb_2O_5-NW, and TT-Nb_2O_5-NW (Figure S3). This material is available free of charge on the Web at: http://www.csj.jp/journals/bcsj/.

References

1 A. Fujishima, K. Honda, *Nature* **1972**, *238*, 37.

2 Reports of photocatalysts enabling overall water splitting or H_2 and/or O_2 production in the presence of sacrificial reagents under UV or visible light irradiation are summarized in the following review; see: A. Kudo, Y. Miseki, *Chem. Soc. Rev.* **2009**, *38*, 253.

3 a) K. Sayama, A. Tanaka, K. Domen, K. Maruya, T. Onishi, *Catal. Lett.* **1990**, *4*, 217. b) H. Liu, R. Nakamura, Y. Nakato, *Electrochem. Solid-State Lett.* **2006**, *9*, G187. c) T. Sreethawong, S. Yoshikawa, *Int. J. Hydrogen Energy* **2006**, *31*, 786. d) T. Mitsuyama, A. Tsutsumi, T. Hata, K. Ikeue, M. Machida, *Bull. Chem. Soc. Jpn.* **2008**, *81*, 401. e) P. S. Lunawat, R. Kumar, N. M. Gupta, *Catal. Lett.* **2008**, *121*, 226. f) K. Maeda, H. Terashima, K. Kase, M. Higashi, M. Tabata, K. Domen, *Bull. Chem. Soc. Jpn.* **2008**, *81*, 927.

4 a) H. Kato, A. Kudo, *Catal. Today* **2003**, *78*, 561. b) H. Kato, K. Asakura, A. Kudo, *J. Am. Chem. Soc.* **2003**, *125*, 3082. c) A. Yamakata, T. Ishibashi, H. Kato, A. Kudo, H. Onishi, *J. Phys. Chem. B* **2003**, *107*, 14383.

5 Previous reports with regard to template-directed synthesis of semiconductor nanotubes are summarized in the following review; see: C. Bae, H. Yoo, S. Kim, K. Lee, J. Kim, M. M. Sung, H. Shin, *Chem. Mater.* **2008**, *20*, 756.

6 a) N. Bao, L. Shen, T. Takata, D. Lu, K. Domen, *Chem. Lett.* **2006**, *35*, 318. b) J. Yu, A. Kudo, *Adv. Funct. Mater.* **2006**, *16*, 2163. c) J. Jitputti, S. Pavasupree, Y. Suzuki, S. Yoshikawa, *Jpn. J. Appl. Phys.* **2008**, *47*, 751.

7 D. A. Bayot, M. M. Devillers, *Inorg. Chem.* **2006**, *45*, 4407.

8 B. D. Yuhas, D. O. Zitoun, P. J. Pauzauskie, R. He, P. Yang, *Angew. Chem., Int. Ed.* **2006**, *45*, 420.

9 a) L. K. Frevel, H. W. Rinn, *Anal. Chem.* **1955**, *27*, 1329. b) F. Holtzberg, A. Reisman, M. Berry, M. Berkenblit, *J. Am. Chem. Soc.* **1957**, *79*, 2039. c) H. Schäfer, R. Gruehn, F. Schulte, *Angew. Chem., Int. Ed. Engl.* **1966**, *5*, 40.

10 a) L. E. Greene, B. D. Yuhas, M. Law, D. Zitoun, P. Yang, *Inorg. Chem.* **2006**, *45*, 7535. b) T. Andelman, Y. Gong, M. Polking, M. Yin, I. Kuskovsky, G. Neumark, S. O'Brien, *J. Phys. Chem. B* **2005**, *109*, 14314.

11 Y. Narendar, G. L. Messing, *Chem. Mater.* **1997**, *9*, 580.

12 a) A. Kudo, A. Tanaka, K. Domen, K. Maruya, T. Onishi, *Bull. Chem. Soc. Jpn.* **1992**, *65*, 1202. b) H. Kominami, K. Oki, M. Kohno, S. Onoue, Y. Kera, B. Ohtani, *J. Mater. Chem.* **2001**, *11*, 604.

13 a) M. Mozetič, U. Cvelbar, M. K. Sunkara, S. Vaddiraju, *Adv. Mater.* **2005**, *17*, 2138. b) E. R. Leite, C. Vila, J. Bettini, E. Longo, *J. Phys. Chem. B* **2006**, *110*, 18088. c) Y. Kobayashi, H. Hata, M. Salama, T. E. Mallouk, *Nano Lett.* **2007**, *7*, 2142. d) C. Yan, D. Xue, *Adv. Mater.* **2008**, *20*, 1055. e) B. Varghese, S. C. Haur, C.-T. Lim, *J. Phys. Chem. C* **2008**, *112*, 10008.